

# OmniSpectra: A Unified Foundation Model for Native Resolution Astronomical Spectra

Md Khairul Islam<sup>1</sup>, Judy Fox<sup>1, 2</sup>

<sup>1</sup>Computer Science Dept, University of Virginia

<sup>2</sup>School of Data Science, University of Virginia

mi3se@virginia.edu, ckw9mp@virginia.edu

## Abstract

We present **OmniSpectra**, the first native-resolution foundation model for astronomy spectra. Unlike traditional models, which are limited to fixed-length input sizes or configurations, OmniSpectra handles spectra of any length at their original size, without resampling or interpolation. Despite the large-scale spectroscopic data from diverse surveys fueling the rapid growth of astronomy, existing foundation models are limited to a fixed wavelength range and specific instruments. OmniSpectra is the first foundation model to learn simultaneously from multiple real-world spectra surveys with different configurations at a large scale. We achieve this by designing a novel architecture with adaptive patching across variable lengths, sinusoidal global wavelength encoding, local positional embeddings through depthwise convolution, and validity-aware self-attention masks. Allowing us to learn multi-scale spatial patterns while skipping attention for invalid patches. Even with a limited training example, OmniSpectra demonstrates excellent zero-shot generalization compared to methods tailored for specific tasks. This transfer learning capability makes this model the state-of-the-art across various astronomy tasks, including source classification, redshift estimation, and properties prediction for stars and galaxies. OmniSpectra reduces the need for training individual models for different tasks from scratch, establishing itself as the next-generation astronomy foundation model.

## Introduction

Astronomy is expanding rapidly, with large-scale surveys like SDSS (Blanton et al. 2017; Kollmeier et al. 2019), Gaia (De Angeli et al. 2023), ALMA (Hunter et al. 2023), the recent Rubin Observatory Legacy Survey of Space and Time (Ivezić et al. 2019), and more. The Multimodal Universe (Audenaert et al. 2024) curated over 100TB of machine learning ready astronomy data. This large and mostly unlabeled data creates a great opportunity to build self-supervised foundation models for learning a unified representation of the universe.

Despite the opportunity for finding millions of unseen asteroids, comets and interstellar objects, most applications rely on task or instrument-specific small models (Smith and Geach 2023; Lanusse et al. 2023). **Spectroscopy**—is the most information-rich modality in astronomy—offers insights into redshift, stellar composition, galactic

kinematics, and chemical abundances. However, current models struggle to scale and generalize across different spectral surveys due to inconsistencies in resolution, wavelength coverage, instrument design, and a lack of labeled data.

Recent foundation models for astronomical spectra (Parker et al. 2024; Leung and Bovy 2024; Koblischke and Bovy 2024; Rizhko and Bloom 2025) are typically pretrained on a single survey or at a fixed resolution, limiting their cross-survey generalization. Extending such models to new instruments requires substantial retraining or building dedicated encoders—contrary to the promise of unified representation learning.

We introduce **OmniSpectra**, a major step toward this goal. It is the **first native-resolution foundation model for astronomical spectra**. By native resolution, we mean a model capable of processing variable lengths of spectra from arbitrary instruments at their original size, without having to truncate or project to a predefined fixed size. OmniSpectra uses a Transformer-based architecture pretrained with a masked modeling objective. Our major contributions are as follows:

- **OmniSpectra**, a self-supervised spectral foundation model pretrained using masked modeling objective. This handles variable-length spectra using validity-aware self-attention to skip padded regions.
- A hybrid attention mechanism, combining global sinusoidal (from wavelengths) and local convolutional positional embeddings, capturing both coarse and fine spectral structures.
- Concurrent pretraining on eight diverse surveys spanning 5.5 million examples, and extendable to any number of datasets.
- State-of-the-art performance across a wide range of classification and regression benchmarks, with strong zero-shot generalization.

## Foundation Models in Astronomy

A variety of deep learning models have been proposed for spectroscopic analysis in astronomy, ranging from autoencoders to supervised regressors and cross-modal encoders.

Table 1: Related works summary on deep Learning for astronomy spectra. SSL: Self-Supervised Learning. The context is the input spectrum or sequence length each model takes at a time. The tasks include input source classification, galaxy or stellar property, and redshift prediction.

Model	Method	Survey	Sample	Context	Param.	Downstream Tasks			
						Source	Galaxy	Stellar	Redshift
OmniSpectra	SSL	DESI EDR, SDSS, APOGEE, VIPER	5.5M	Native	42.5M	✓	✓	✓	✓
AstroCLIP		DESI EDR	221K	8000	350M		✓		✓
Specformer		DESI EDR	221K	8000	43.2M		✓		✓
Leung and Bovy (2024)		APOGEE, GAIA	400K	64	8.8M			✓	
GalSpecNet	Supervised	SDSS, LAMOST	119K	2575	465 K		✓		
Spender		SDSS	650K	3921	28.8K		✓		
SpectraFM		APOGEE	90K	512	11.8M			✓	

Spender (Melchior et al. 2023) is a convolutional autoencoder augmented with attention for modeling galaxy spectra. This has been extended to unsupervised outlier detections (Liang et al. 2023). GalSpecNet (Wu et al. 2024) is a CNN-based classifier designed to predict galaxy morphology directly from SDSS spectra. The model significantly outperforms classical machine learning baselines, but needs modification for different input sizes. Spectral Transformer (SPT) (Zhang et al. 2024) predicts stellar ages and masses from red giant spectra, trained on 3,880 samples from LAMOST. This targets a specific supervised task and is trained on a relatively small dataset.

Leung and Bovy (2024) proposed a Transformer-based model that predicts stellar properties from tabular summaries of low-resolution spectra (e.g., from Gaia). Though applicable to multi-survey data, this model uses processed metadata, not raw spectra. SpectraFM (Koblischke and Bovy 2024) extends this work to high-resolution spectra, using synthetic stellar spectra for pretraining and fine-tuning on real APOGEE data. However, SpectraFM processes spectra in fixed-length windows of 512 tokens, averaging predictions across chunks. This constrains it to fixed-resolution inputs and limits generalization.

AstroCLIP (Parker et al. 2024) presents the first cross-modal foundation model for galaxies with image and spectrum data. Specformer is the unimodal spectrum encoder of AstroCLIP. They use a fixed sequence length, since it was only trained on the DESI EDR spectra. AstroM3 (Rizhko and Bloom 2025) used the GalSpecNet (Wu et al. 2024) as the spectra encoder and aligned the embeddings with time-series and metadata using CLIP (Contrastive Language-Image Pretraining). However, they require all modalities, and the input size is fixed as GalSpecNet.

Previous approaches rely on supervised learning or are pretrained on specific datasets, limiting their ability to handle variable-resolution spectra from diverse instruments. In contrast, our work is the first to address this challenge using unsupervised learning directly from raw spectral data.

## OmniSpectra

This section provides the details of our proposed model and its design. Figure 1 illustrates a brief overview of the architecture.

### Tokenization

Let each observed 1D spectrum be denoted as a sequence of flux values with associated wavelengths.

$$\{(\lambda_i, f_i)\}_{i=1}^L, \quad L \in \mathbb{N}.$$

where  $\lambda_i$  is the wavelength and  $f_i$  is the corresponding flux measurement. Due to variability in instrument resolution and observation length,  $L$  varies across samples. We partition the spectrum into partially overlapping *patches* of fixed size  $p$  after normalization. Overlapping is used to enhance learning local structures. We also add the mean ( $\mu_t$ ) and standard deviation ( $\sigma_t$ ) of the flux values to the token sequence.

$$\mathbf{x}_t = [\mu_t, \sigma_t, f_{t,1}, f_{t,2}, \dots, f_{t,p}] \in \mathbb{R}^{p+2},$$

For a spectrum split into  $T$  such patches, the full input sequence becomes:

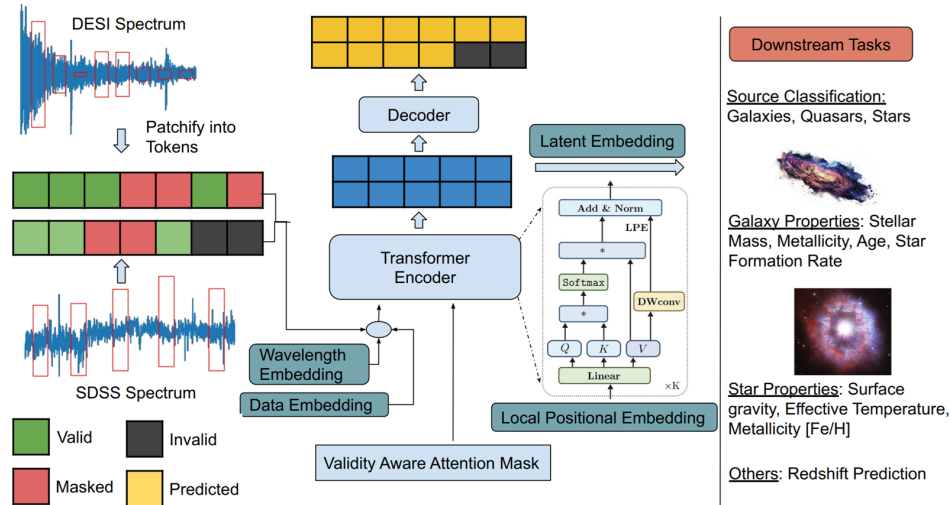
$$\mathbf{X} = \begin{bmatrix} \mathbf{x}_1 \\ \mathbf{x}_2 \\ \vdots \\ \mathbf{x}_T \end{bmatrix} \in \mathbb{R}^{T \times (p+2)}.$$

We design a collator to make the sequence lengths within a single batch the same. This supports variable-length sequences during training. A binary mask  $M \in \{0, 1\}^T$  tracks which patches are valid or padded.

### Masking

To train the model using a reconstruction objective, we adopt a *contiguous chunk masking scheme*. This strategy masks coherent spans of input tokens—corresponding to physically contiguous wavelength ranges—encouraging the model to capture both local spectral structure and long-range dependencies.

Figure 1: OmniSpectra: model architecture overview. Left: Spectra tokenization and masking steps. Middle: The Masked Transformer architecture with wavelength and local positional embedding. Right: Downstream tasks



Given input token sequence  $\mathbf{X}$ , let  $\gamma \in (0, 1)$  be the *mask ratio*, the fraction of the input tokens to be masked during training. We partition the sequence into  $N$  contiguous, non-overlapping chunks of width  $w$ , where

$$w = \lfloor 2.5 \times p \rfloor, \quad N = \left\lfloor \frac{T}{2w} \right\rfloor$$

With  $p$  denoting the patch size used in the tokenization step. Among the  $N$  chunks, we randomly select  $M = \lfloor \gamma N \rfloor$  non-overlapping chunks to be masked, ensuring that no two masked chunks are adjacent. We use a **mask ratio of 0.75** throughout our experiments. This masking procedure is applied independently for each spectrum in the batch.

Each selected chunk corresponds to a subsequence  $\mathbf{x}_{s:s+w}$ , where  $s$  is a randomly chosen start index within the designated interval. The masked sequence  $\tilde{\mathbf{X}} \in \mathbb{R}^{T \times (p+2)}$  is formed by zeroing out the selected regions:

$$\tilde{\mathbf{x}}_t = \begin{cases} \mathbf{0} & \text{if } t \in \bigcup_{i=1}^M [s_i, s_i + w) \\ \mathbf{x}_t & \text{otherwise} \end{cases}$$

## Embedding

To represent variable-length 1D spectral inputs in a latent space suitable for transformer-based processing, we combine a *learned data projection* with a *sinusoidal encoding of spectral wavelength* in the embedding. This design enables the model to integrate both spectral content and global positional information at each token location.

**Data Embedding:** The tokenized and collated input sequence ( $\mathbf{X}$ ) is first projected to a fixed embedding dimension  $D_{\text{emb}}$ :

$$\mathbf{z}_t = \mathbf{W}_{\text{data}} \mathbf{X} + \mathbf{b}_{\text{data}}, \quad \mathbf{W}_{\text{data}} \in \mathbb{R}^{D_{\text{emb}} \times (p+2)}$$

This produces a projected token sequence  $\mathbf{Z} = [\mathbf{z}_1, \dots, \mathbf{z}_T] \in \mathbb{R}^{B \times T \times D_{\text{emb}}}$ , where  $B$  is the batch size.

To stabilize training and avoid large initial activations, we initialize the weights using a truncated normal distribution:

$$\mathbf{W}_{\text{data}} \sim \mathcal{N} \left( 0, \frac{1}{D_{\text{emb}}} \right), \quad \text{truncated to } [-3\sigma, +3\sigma]$$

**Sinusoidal Wavelength Encoding:** To retain physically meaningful information about the central wavelength of each patch, we inject a sinusoidal encoding based on the mean wavelength  $\lambda_t \in \mathbb{R}$  of the patch  $t$ . Following Vaswani et al. (2017), this is defined as:

$$\mathbf{p}_t^{(2i)} = \sin(\lambda_t \cdot \omega_i), \quad \mathbf{p}_t^{(2i+1)} = \cos(\lambda_t \cdot \omega_i)$$

where  $i = 0, 1, \dots, \lfloor \frac{D_{\text{emb}}}{2} \rfloor - 1$ , and  $\omega_i = 10000^{-\frac{2i}{D_{\text{emb}}}}$  controls the frequency scale. Let  $\mathbf{\Lambda} \in \mathbb{R}^{B \times T}$  denote the matrix of patch-wise mean wavelengths. The full sinusoidal encoding tensor  $\mathbf{P} \in \mathbb{R}^{B \times T \times D_{\text{emb}}}$ , is thus constructed via:

$$\mathbf{PE}_{\text{global}} = \text{sinusoidal\_encoding}(\mathbf{\Lambda}, D_{\text{emb}})$$

Unlike absolute or relative positional indices used in natural language processing, this encoding reflects physical wavelength values, which may vary non-uniformly and span arbitrary ranges across instruments. The final token representation is computed as:

$$\mathbf{Z} = \mathbf{Z} + PE_{\text{global}}$$

## Transformer Block

We adopt a Transformer backbone equipped with Flash Attention for efficient memory scaling and computational throughput. To handle native-resolution, variable-length spectral sequences, we incorporate two key architectural enhancements: (i) *validity-aware attention mechanism* that restricts attention computation to valid (non-padded) tokens

and (ii) *local positional embedding module* that captures short-range spectral patterns.

Each Transformer layer follows a standard pre-activation residual structure comprising a multi-head self-attention (MHSA) block and a feed-forward network (FFN):

$$\begin{aligned}\mathbf{Z}' &= \mathbf{Z} + \text{MHA}(\text{LayerNorm}(\mathbf{Z}), \mathcal{A}) \\ \mathbf{Z}_{\text{out}} &= \mathbf{Z}' + \text{FFN}(\text{LayerNorm}(\mathbf{Z}')).\end{aligned}$$

We previously introduced a *validity mask*  $\mathbf{M} \in \{0, 1\}^{B \times T}$  where  $M_{b,t} = 1$  indicates the token  $t$  in batch index  $b$  is a real (non-padded) patch. The additive attention mask  $\mathcal{A} \in \mathbb{R}^{B \times 1 \times T \times T}$  is constructed from this binary validity signal:

$$\mathcal{A}_{b,1,i,j} = \begin{cases} 0 & \text{if } M_{b,i} = M_{b,j} = 1 \\ -\infty & \text{otherwise} \end{cases}$$

This ensures that attention is computed *only among valid tokens* and allows the model to scale to variable-length sequences, while preserving computational efficiency.

**Local Positional Embedding** To robustly capture fine-grained spectral structures across varying instrumental resolutions, we introduce a local positional embedding mechanism that encodes inductive biases about neighborhood continuity directly into the attention computation. While the sinusoidal encoding provides global wavelength information, local correlations—such as emission/absorption line shapes—require explicitly modeling short-range spatial dependencies. We achieve this by augmenting the value tensor  $\mathbf{V}$  with a depthwise convolution, applied independently across attention heads and channels:

$$\mathbf{PE}_{\text{local}} = \text{Conv1D}_{\text{depthwise}}(\mathbf{V}),$$

where  $\text{Conv1D}_{\text{depthwise}}$  is a grouped convolution with kernel size 3 and group count =  $d_h$ . This convolution captures localized features while preserving the structure of multi-head attention. We then enhance attention output as:

$$\mathbf{Y} = \mathbf{Y}_{\text{att}} + \mathbf{PE}_{\text{local}}.$$

Finally, the outputs from all heads are concatenated and projected via a linear transformation:

$$\text{MHA}(\mathbf{Z}) = \text{Concat}(\mathbf{Y}_1, \dots, \mathbf{Y}_H) \mathbf{W}^O.$$

## Reconstruction Loss

The output of the final Transformer layer  $\mathbf{Z}_{\text{final}} \in \mathbb{R}^{B \times T \times d}$  is passed through a linear head to predict the masked tokens:

$$\hat{\mathbf{X}} = \mathbf{Z}_{\text{final}} \mathbf{W}_{\text{out}} + \mathbf{b}_{\text{out}}, \quad \hat{\mathbf{X}} \in \mathbb{R}^{B \times T \times (p+2)}.$$

Let  $\mathbf{Y} \in \mathbb{R}^{B \times T \times D_{\text{in}}}$  denote the ground truth input and  $\hat{\mathbf{Y}} \in \mathbb{R}^{B \times T \times D_{\text{in}}}$  the model's reconstruction. The loss is computed **only over valid masked positions**, using a mean squared error (MSE) formulation:

$$\mathcal{L}_{\text{recon}} = \frac{1}{\sum_{b,t} m_{b,t}} \sum_{b=1}^B \sum_{t=1}^T m_{b,t} \cdot \|\hat{\mathbf{y}}_{b,t} - \mathbf{y}_{b,t}\|_2^2$$

where  $m_{b,t} = 1$  if token  $t$  in sample  $b$  was masked, and 0 otherwise. This encourages the model to infer missing spectral information purely from the unmasked context.

## Downstream Linear Probe

For downstream tasks, we optionally fine-tune the pretrained encoder and append a linear prediction head. Given the encoded patch embeddings  $\mathbf{Z} \in \mathbb{R}^{T \times d}$ , where  $d$  is the embedding dimension. We first compute the mean pooled embedding representation across the token sequence:

$$\mathbf{Z}_{\text{avg}} = \frac{1}{T} \sum_{t=1}^T \mathbf{Z}_t$$

The pooled embedding is then normalized and passed through a linear output head to produce prediction logits:

$$\hat{\mathbf{y}} = \mathbf{W}_{\text{head}}(\text{LayerNorm}(\mathbf{Z}_{\text{avg}})) + \mathbf{b}_{\text{head}}$$

For **regression** tasks, such as stellar parameter or redshift estimation, we normalize the target values during training to stabilize optimization:

$$\mathbf{y}_{\text{norm}} = \frac{\mathbf{y} - \boldsymbol{\mu}}{\boldsymbol{\sigma} + \epsilon},$$

where  $\boldsymbol{\mu}, \boldsymbol{\sigma}$  are target means and standard deviations estimated from the training batch. We minimize the mean squared error loss:

$$\mathcal{L}_{\text{reg}} = \frac{1}{N} \sum_{i=1}^N \|\hat{\mathbf{y}}_i - \mathbf{y}_{\text{norm},i}\|_2^2.$$

For **classification** tasks (e.g., source type), we use the same mean-pooled embedding and linear head, trained with class-weighted cross-entropy.

## Experimental Setup

### Dataset

We pretrain OmniSpectra on a diverse collection of **publicly available** spectroscopic surveys that span a wide range of instruments, resolutions, and scientific targets. This enables robust cross-domain generalization. These datasets have also been used in many deep learning astronomy applications (Smith and Geach 2023).

The Dark Energy Spectroscopic Instrument (**DESI**, (Adame et al. 2024) maps the large-scale structure of the universe and is among the most ambitious spectroscopic surveys to date. We utilize the DESI Early Data Release (EDR) processed by Audenaert et al. (2024), which was also used to pretrain AstroCLIP (Parker et al. 2024).

The Sloan Digital Sky Survey (**SDSS**, (York et al. 2000)) is one of the most influential astronomical surveys, providing high-quality spectra and imaging of millions of celestial objects, spanning over two decades of observations

Table 2: Dataset description with number of samples, maximum context size, and wavelength range.

Survey	Samples	Seq. Length	Wavelength (Å)
DESI EDR	1M	7781	3600 - 9800
SDSS Legacy	806K	3866	3786 - 9219
BOSS	2.03M	4661	3568 - 10387
eBOSS	1.09M	4616	3583 - 10370
SEGUE1	213K	3851	3800 - 9221
SEGUE2	111K	3866	3786 - 9219
APOGEE	102K	7514	15152 - 16943
VIPERS	91K	557	5514 - 9484

(Eisenstein et al. 2011; Blanton et al. 2017). We collect all SDSS (18th data release) optical spectroscopic data from (Audenaert et al. 2024), including its subsets:

- SDSS Legacy survey
- SEGUE-1, SEGUE-2 (Stellar surveys)
- BOSS, and eBOSS (galaxy and quasar surveys)

The “VIMOS Public Extragalactic Redshift Survey” (**VIPERS**, (Scodéggi et al. 2018)) dataset contains optical spectra of galaxies in  $0.5 < z < 1.0$  range taken at the center of each galaxy. The Apache Point Observatory Galactic Evolution Experiment (**APOGEE**, (Abdurro’uf et al. 2022)) is a high-resolution and high signal-to-noise stellar spectroscopic survey at near infrared H-band wavelength region. We use the APOGEE 17th data release used in SpectraFM (Koblischke and Bovy 2024).

## Self-Supervised Pretraining

We design a unified and scalable training pipeline capable of jointly learning from diverse spectroscopic surveys. We use all eight datasets in Table 2 in a single training, so a batch may contain samples from multiple sources and shapes. Thus allowing the model to encounter spectra from multiple instruments and resolutions concurrently. The files are in HDF5 format.

We use a batch size of 128 and train with 4 CPU workers and a prefetch factor of 2 to optimize I/O throughput. The input spectra are tokenized using a patch size of 20 with an overlap of 10 flux points, and normalized independently for each instance. The validation set is constructed as a random 1% subsample of the full training corpus (55K spectra) and is kept fixed throughout training. A random seed of 42 was used for pretraining reproducibility.

OmniSpectra is implemented in PyTorch using the Lightning framework to leverage efficient GPU acceleration and distributed training. We employ Distributed Data Parallel (DDP) across 4 NVIDIA A100 GPUs, 20 Intel Xeon CPU cores with 48GB RAM per device in a single node. We train the model for a maximum of 2 million steps for 48 hours. Model checkpoints and validation metrics are recorded every 800 steps. We use an embedding dimension of 768, with 6 encoder layers and 6 self-attention heads, totaling 42.6 million parameters. We use a masking ratio of 0.75.

Training optimization is performed using the AdamW optimizer with a learning rate of  $10^{-4}$ , weight decay 0.01, and  $\beta$ -parameters [0.9, 0.95]. We apply gradient clipping at 1.0 to prevent instabilities during training. The learning rate is annealed using PyTorch’s CosineAnnealingWarmRestarts scheduler, with  $T_0 = 200,000$  and  $\eta_{min} = 10^{-6}$ . The model is trained with a mean squared error loss between the original token flux and predicted token flux at the masked regions.

We tuned the following hyper-parameters :

- learning rate:  $[10^{-4}, 5 \times 10^{-4}, 10^{-5}]$
- batch size: [64, 128]
- embed dimension: [512, 768]
- transformer layers: [4, 6, 8]
- attention heads: [4, 6, 8]

## Downstream Fine-Tuning

**Each downstream experiment is run five times and we report the average results here.** We sample 20,000 examples from each dataset, randomly selecting 50% as training and 50% as the test dataset. The probe model is a linear head wrapped over the pretrained model. We use a batch size of 64 and a learning rate of  $10^{-4}$  during the downstream tuning. The supervised models are trained for 10 epochs, with a learning rate of  $10^{-3}$ . For **zero-shot learning**, we tune the pretrained models for 100 steps/batches. For **few-shot learning**, we train the pretrained models for 500 steps. These numbers are arbitrarily chosen.

## Baselines

**AstroCLIP** (Parker et al. 2024) is a state-of-the-art multimodal foundation model trained on galaxy spectra and images. Its unimodal spectral encoder, **Specformer**, is also evaluated independently. **SpectraFM** (Koblischke and Bovy 2024) is a stellar foundation model pretrained on synthetic spectra and fine-tuned on APOGEE for stellar property estimation, extending the architecture of Leung and Bovy (2024). Since it is only pretrained on star spectra, we only use it for star property estimation. **GalSpecNet** (Wu et al. 2024) is a CNN-based supervised model and is used as the spectra encoder in AstroM<sup>3</sup>. **Spender** (Melchior et al. 2023) is a convolutional autoencoder with attention. **The supervised models are individually trained from scratch for each dataset and task.** Their architecture is also adjusted to support that input size (final linear layer, kernel size).

## Results

### Galaxy Property Estimation

Estimating galactic properties from spectra is a key astronomy task. PROVABGS (Hahn et al. 2023) provides probabilistic estimates of galaxy properties, including log stellar mass ( $\log M_*$ ), star formation rate ( $sSFR$ ), mass-weighted stellar metallicity ( $Z_{MW}$ ), and mass-weighted stellar age ( $t_{age}$ ) for the DESI Bright Galaxy Survey (BGS). We match the cross-matched AstroCLIP image-spectra pairs with the PROVABGS

Table 3: Mean-Squared Error ( $\downarrow$ ) of star property estimation on the SDSS dataset and its subsets. We report the weighted average across the targets. The best and second-best results are in **bold** and underline. OmniSpectra significantly outperforms other foundation models and even custom supervised models with little tuning.

Model	Method	SDSS	BOSS	eBOSS	SEGUE1	SEGUE2
OmniSpectra	Zero-shot	0.487	0.685	0.735	0.473	0.316
	Few-shot	<b>0.431</b>	<b>0.648</b>	<b>0.671</b>	<b>0.401</b>	<b>0.294</b>
AstroCLIP	Zero-shot	0.540	0.806	0.842	0.644	0.454
	Few-shot	0.506	0.767	0.794	0.534	0.359
Specformer	Zero-shot	0.561	0.796	0.849	0.578	0.518
	Few-shot	0.516	0.766	0.787	0.540	0.401
SpectraFM	Zero-shot	1.223	1.170	1.012	1.072	1.078
	Few-shot	1.084	1.161	1.046	1.052	0.965
GalSpecNet	Supervised	<u>0.443</u>	<u>0.663</u>	<u>0.693</u>	<b>0.401</b>	0.302
Spender	Supervised	0.480	0.727	0.766	<u>0.472</u>	0.356

dataset using the DESI target IDs. Then remove spurious entries by only selecting entries for which  $M_* > 0$  and  $mag_g, mag_r, mag_z > 0$ . This leaves 105,159 samples, which we split using an 80/20 train-test split for training and evaluation. This setup follows Parker et al. (2024).

Table 4: Galaxy property estimation using  $R^2$  score ( $\uparrow$ ). The best and second-best results are in **bold** and underline. OmniSpectra performs best across the targets.

Model	Method	$M_*$	$Z_{MW}$	$t_{age}$	$sSFR$
OmniSpectra	Zero-shot	0.86	0.58	0.43	0.64
	Few-shot	<b>0.88</b>	<b>0.64</b>	<b>0.50</b>	<b>0.71</b>
AstroCLIP	Zero-shot	0.87	0.57	0.43	0.63
	Few-shot	<b>0.88</b>	0.58	0.43	0.64
Specformer	Zero-shot	0.84	0.57	0.38	0.62
	Few-shot	<b>0.88</b>	<b>0.64</b>	<u>0.47</u>	<u>0.69</u>
GalSpecNet	Supervised	<u>0.87</u>	0.61	0.45	0.63
Spender	Supervised	0.85	<u>0.62</u>	0.43	0.67

Following the AstroCLIP experiment setup, for zero-shot training, we use k-NN to regress  $[\log M_*, \log Z_{MW}, t_{age}, \log sSFR]$ ; for few-shot training, we use a single-hidden-layer MLP with hidden dimension 32 to perform the same regression. Table 4 shows that **our model performs better or similar to the current state-of-the-art model**.

## Stellar Property Estimation

For stellar property estimation, we use the **Elodie-based parameters** present in the SDSS spectroscopic dataset and its subsets. The target properties are: (i) **TEFF**: Effective temperature, (ii) **Surface gravity** ( $\log g$ ), and (iii) **Metallicity** ([Fe/H]). These labels are derived by fitting derived spectra to high-resolution templates from the ELODIE spectral library. They serve as a reliable ground truth for evaluating stellar property estimation models. Although SDSS also contains galactic spectra, these values are only defined for stars.

Table 3 presents the mean squared error (MSE) on test set, averaged across the three regression targets. The supervised

models are trained for 10 epochs. The pretrained models are fine-tuned using a linear head for 100 and 500 steps (batch size 64) for zero-shot and few-shot learning, respectively.

**OmniSpectra achieves the lowest error across all cases.** Notably, its zero-shot performance often surpasses the supervised and few-shot baselines, underscoring the quality of the learned representations.

## Source Classification

Classifying the spectra source is a common astronomy downstream task. We evaluate source type classification on the SDSS dataset and its subsets. The supervised models are trained for 10 epochs. The pretrained models are fine-tuned using a linear head for 100 and 500 steps (batch size 64) for zero-shot and few-shot learning respectively. Segue1 and Segue2 are excluded since they only focus on star sources. Table 5 shows that the classes are highly imbalanced. We address this by using class weights in classification loss and training data sampling. The class weight is calculated from the training sample by taking the inverse of the normalized square root of their counts. This is used in the training data to create a random weighted sampler. These weights are passed to the cross-entropy loss in the linear probing model. The test data stays unchanged, reflecting the original data distribution.

Table 5: Source class distribution in the SDSS dataset.

Source	SDSS	BOSS	eBOSS
Galaxy	0.78	0.73	0.51
Quasar	0.06	0.14	0.39
Star	0.16	0.13	0.09

Table 6 shows that OmniSpectra outperforms other models in all cases. We chose F1-score over other metrics since the dataset is highly imbalanced. Despite the class imbalance, OmniSpectra performs robustly across all classes.

## Redshift Prediction

Redshift estimation uses the cross-matched data between the AstroCLIP (Parker et al. 2024) image-spectra pair dataset

Figure 2: Few-shot redshift prediction for galaxy spectrum (here  $Z$  represents redshift). OmniSpectra outperforms the current best models in R2-score ( $\uparrow$ ).

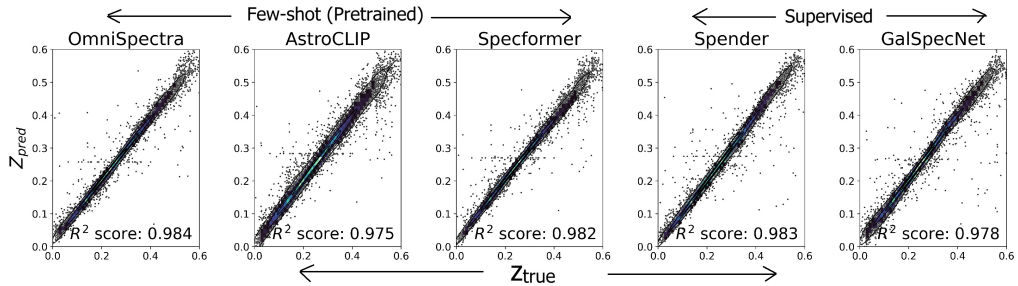


Table 6: F1-score ( $\uparrow$ ) on spectra source classification test results. The best and second-best results are in **bold** and underline. **OmniSpectra performs the best across targets, with excellent zero-shot performance.**

	Model	Method	Galaxy	Quasar	Star
SDSS	<b>OmniSpectra</b>	Zero-shot	0.984	0.867	0.957
		Few-shot	<b>0.990</b>	<b>0.915</b>	<b>0.958</b>
	AstroCLIP	Zero-shot	0.975	0.812	0.829
		Few-shot	0.985	<u>0.896</u>	0.925
	Specformer	Zero-shot	0.878	0.566	0.479
		Few-shot	0.976	0.866	0.895
BOSS	<b>OmniSpectra</b>	Supervised	<u>0.988</u>	0.888	<u>0.957</u>
		Supervised	0.986	0.885	0.948
	AstroCLIP	Zero-shot	<b>0.988</b>	<b>0.913</b>	<b>0.955</b>
		Few-shot	<u>0.984</u>	0.889	<u>0.942</u>
	Specformer	Zero-shot	0.952	0.854	0.725
		Few-shot	0.956	0.851	0.780
eBOSS	<b>OmniSpectra</b>	Zero-shot	<b>0.988</b>	0.894	<b>0.958</b>
		Few-shot	<u>0.979</u>	<b>0.929</b>	<u>0.910</u>
	AstroCLIP	Zero-shot	0.853	0.825	0.573
		Few-shot	0.878	0.885	0.728
	Specformer	Zero-shot	0.953	0.690	0.72
		Few-shot	0.976	0.672	0.818
	GalSpecNet	Supervised	0.935	<u>0.921</u>	0.895
		Supervised	0.900	0.892	0.837

and the PROVABGS (105,159 labeled samples), and follows the same evaluation setup. Figure 2 shows the few-shot performance that uses an MLP model with hidden ReLU layers [64, 64], a dropout rate of 0.1, and a learning rate of 1e-3 for 10 epochs with batch size 64. OmniSpectra performs best among the models, closely followed by the supervised model Spender.

### Ablation Study

To evaluate the contribution of each architectural component, we perform an ablation study by removing one module at a time and retraining the model with

the same self-supervised learning (SSL) setup. Table 7 reports the validation reconstruction loss (MSE) for each variant. The full OmniSpectra model achieves the lowest reconstruction error, confirming the effectiveness of all three components. The global wavelength embedding has the most significant effect. This aligns with expectations, as spectra from different surveys span diverse wavelength ranges. Embedding this physical context allows the model to better align and interpret the flux measurements.

Method	Reconstruction Loss (MSE) ( $\downarrow$ )
OmniSpectra	<b>0.505</b>
w/o Local Positional Embedding	0.531
w/o Wavelength Embedding	0.903
w/o Validity Attention Mask	<u>0.525</u>

Table 7: Ablation study on key architectural components.

## Conclusion

We introduce OmniSpectra, a strong-performing foundation model for astronomical spectroscopy, enabling a unified and scalable approach to deep learning across diverse surveys. OmniSpectra achieves state-of-the-art performance across many downstream tasks, spanning heterogeneous datasets and distributions. Notably, it maintains strong performance in both zero and few-shot settings, significantly reducing the reliance on labeled data. This establishes OmniSpectra as a practical and generalizable alternative to existing supervised approaches. Our work represents a significant advancement toward universal representation learning in astronomy, enabling the leveraging of vast amounts of unlabeled spectral data from instruments with varying resolutions and configurations.

## Acknowledgement

This work is partly supported by NSF-Simons AI Institute for Cosmic Origins (CosmicAI: Grant 2421782) Seed Grant. NSF CF-1918626 Expeditions: Collaborative Research: Global Pervasive Computational Epidemiology, and NSF Grant 2200409 for CyberTraining: CIC: CyberTraining for Students and Technologies from Generation Z. NSF -

2504401 OAC Core: RINAS: Data I/O CyberInfrastructure for Extreme-scale Foundation Model and Generative AI Training on HPC.

## References

Abdurro'uf, N.; Accetta, K.; Aerts, C.; Silva Aguirre, V.; Ahumada, R.; Ajgaonkar, N.; Filiz Ak, N.; Alam, S.; Allende Prieto, C.; Almeida, A.; et al. 2022. The seventeenth data release of the Sloan Digital Sky Survey: Complete release of Manga, MaStar, and Apogee-2 data. *The Astrophysical Journal Supplement Series*, 259(2).

Adame, A.; Aguilar, J.; Ahlen, S.; Alam, S.; Aldering, G.; Alexander, D.; Alfarsy, R.; Prieto, C. A.; Alvarez, M.; Alves, O.; et al. 2024. The early data release of the dark energy spectroscopic instrument. *The Astronomical Journal*, 168(2): 58.

Audenaert, J.; Bowles, M.; Boyd, B. M.; Chemaly, D.; Cherinka, B.; Ciucă, I.; Cranmer, M.; Do, A.; Grayling, M.; Hayes, E. E.; et al. 2024. The Multimodal Universe: Enabling Large-Scale Machine Learning with 100TB of Astronomical Scientific Data. *arXiv preprint arXiv:2412.02527*.

Blanton, M. R.; Bershadsky, M. A.; Abolfathi, B.; Albareti, F. D.; Prieto, C. A.; Almeida, A.; Alonso-García, J.; Anders, F.; Anderson, S. F.; Andrews, B.; et al. 2017. Sloan digital sky survey IV: Mapping the Milky Way, nearby galaxies, and the distant universe. *The Astronomical Journal*, 154(1): 28.

De Angeli, F.; Weiler, M.; Montegriffo, P.; Evans, D. W.; Riello, M.; Andrae, R.; Carrasco, J.; Busso, G.; Burgess, P.; Cacciari, C.; et al. 2023. Gaia Data Release 3-Processing and validation of BP/RP low-resolution spectral data. *Astronomy & Astrophysics*, 674: A2.

Eisenstein, D. J.; Weinberg, D. H.; Agol, E.; Aihara, H.; Prieto, C. A.; Anderson, S. F.; Arns, J. A.; Aubourg, É.; Bailey, S.; Balbinot, E.; et al. 2011. SDSS-III: Massive spectroscopic surveys of the distant universe, the milky way, and extra-solar planetary systems. *The Astronomical Journal*, 142(3): 72.

Hahn, C.; Wilson, M. J.; Ruiz-Macias, O.; Cole, S.; Weinberg, D. H.; Moustakas, J.; Kremin, A.; Tinker, J. L.; Smith, A.; Wechsler, R. H.; et al. 2023. The DESI bright galaxy survey: Final target selection, design, and validation. *The Astronomical Journal*, 165(6): 253.

Hunter, T. R.; Indebetouw, R.; Brogan, C. L.; Berry, K.; Chang, C.-S.; Francke, H.; Geers, V. C.; Gómez, L.; Hibbard, J. E.; Humphreys, E. M.; et al. 2023. The ALMA interferometric pipeline heuristics. *Publications of the Astronomical Society of the Pacific*, 135(1049): 074501.

Ivezić, Ž.; Kahn, S. M.; Tyson, J. A.; Abel, B.; Acosta, E.; Allsman, R.; Alonso, D.; AlSayyad, Y.; Anderson, S. F.; Andrew, J.; et al. 2019. LSST: from science drivers to reference design and anticipated data products. *The Astrophysical Journal*, 873(2): 111.

Koblischke, N.; and Bovy, J. 2024. SpectraFM: Tuning into Stellar Foundation Models. *arXiv preprint arXiv:2411.04750*.

Kollmeier, J.; Anderson, S.; Blanc, G.; Blanton, M.; Covey, K.; Crane, J.; Drory, N.; Frinchaboy, P.; Froning, C.; Johnson, J.; et al. 2019. SDSS-V pioneering panoptic spectroscopy. *Bulletin of the American Astronomical Society*.

Lanusse, F.; et al. 2023. The Dawes Review 10: The impact of deep learning for the analysis of galaxy surveys. *Publications of the Astronomical Society of Australia*, 40: e001.

Leung, H. W.; and Bovy, J. 2024. Towards an astronomical foundation model for stars with a transformer-based model. *Monthly Notices of the Royal Astronomical Society*, 527(1): 1494–1520.

Liang, Y.; Melchior, P.; Hahn, C.; Shen, J.; Goulding, A.; and Ward, C. 2023. Outlier Detection in the DESI Bright Galaxy Survey. *The Astrophysical Journal Letters*, 956(1): L6.

Melchior, P.; Liang, Y.; Hahn, C.; and Goulding, A. 2023. Autoencoding galaxy spectra. i. architecture. *The Astronomical Journal*, 166(2): 74.

Parker, L.; Lanusse, F.; Golkar, S.; Sarra, L.; Cranmer, M.; Bietti, A.; Eickenberg, M.; Krawezik, G.; McCabe, M.; Morel, R.; et al. 2024. AstroCLIP: a cross-modal foundation model for galaxies. *Monthly Notices of the Royal Astronomical Society*, 531(4): 4990–5011.

Rizhko, M.; and Bloom, J. S. 2025. AstroM3: A Self-supervised Multimodal Model for Astronomy. *The Astronomical Journal*, 170(1): 28.

Scodellaggio, M.; Guzzo, L.; Garilli, B.; Granett, B.; Bolzonella, M.; De La Torre, S.; Abbas, U.; Adami, C.; Arnouts, S.; Bottini, D.; et al. 2018. The VIMOS public extragalactic redshift survey (Vipers)-full spectroscopic data and auxiliary information release (PDR-2). *Astronomy & Astrophysics*, 609: A84.

Smith, M. J.; and Geach, J. E. 2023. Astronomia ex machina: a history, primer and outlook on neural networks in astronomy. *Royal Society Open Science*, 10(5): 221454.

Vaswani, A.; Shazeer, N.; Parmar, N.; Uszkoreit, J.; Jones, L.; Gomez, A. N.; Kaiser, Ł.; and Polosukhin, I. 2017. Attention is all you need. *Advances in neural information processing systems*, 30.

Wu, Y.; Tao, Y.; Fan, D.; Cui, C.; and Zhang, Y. 2024. Galaxy spectral classification and feature analysis based on convolutional neural network. *Monthly Notices of the Royal Astronomical Society*, 527(1): 1163–1176.

York, D. G.; Adelman, J.; Anderson Jr, J. E.; Anderson, S. F.; Annis, J.; Bahcall, N. A.; Bakken, J.; Barkhouser, R.; Bastian, S.; Berman, E.; et al. 2000. The Sloan Digital Sky Survey: Technical summary. *The Astronomical Journal*, 120(3): 1579.

Zhang, M.; Wu, F.; Bu, Y.; Li, S.; Yi, Z.; Liu, M.; and Kong, X. 2024. SPT: Spectral transformer for age and mass estimations of red giant stars. *Astronomy & Astrophysics*, 683: A163.